

Efficiency of photonic state tomography affected by fiber attenuation

Artur Czerwinski* and Jakub Szlachetka

*Institute of Physics, Faculty of Physics, Astronomy and Informatics
Nicolaus Copernicus University in Toruń, ul. Grudziadzka 5, 87-100 Toruń, Poland*

In this article, we investigate the efficiency of photonic state tomography in the presence of fiber attenuation. The quantum state is reconstructed from photon counts obtained for symmetric informationally complete POVMs. The number of photons that reach the detectors is numerically modeled by the binomial distribution, which describes the loss of light caused by the medium. This approach allows us to study the quality of state tomography versus the length of the fiber. In particular, we focus on entangled qubits and qutrits, which are sent through fibers of different lengths. The amount of entanglement detected by the measurement scheme is quantified and presented on graphs. The results demonstrate how the quality of photonic tomography depends on the distance between the source and the receiver.

Keywords: quantum state tomography, photonic tomography, entangled qutrits, single-photon counting, fiber attenuation, negativity

I. INTRODUCTION

Quantum key distribution (QKD) relies on exchanging a secure key between two distant parties through a non-trusted communication channel [1]. The most common implementation of QKD is based on using single photons as a carrier of a quantum cryptographic key [2–4]. In other protocols, the security of the QKD cryptographic system is guaranteed by the entanglement of the state used to encode the cryptographic key [5]. QKD systems are built on the existing communication channels utilized in modern telecommunication to increase the utility of such systems. The most universal channel for transmitting information is the optical fiber network. Losses in an optical fiber depend exponentially on the length L of the channel used and the attenuation factor, α , which is $\alpha = 0.2$ dB/km for a standard telecommunication fiber for wavelength 1550 nm. Fiber optic losses are mainly due to material absorption. When the distance to exchange cryptographic keys is above 300 km, the losses become significant [6–8]. This is related to the inability to duplicate the entangled states used to exchange the cryptographic key because of the no-cloning theorem [9].

To investigate the impact of fiber attenuation on photon transmission, we implement quantum state tomography (QST), which allows us to obtain the density matrix representing the quantum state from measurable data [10]. Methods of QST are commonly utilized to reconstruct the state of photons produced by a source [11, 12]. Different characteristics of a photonic state can be determined if its density matrix is reconstructed. More specifically, for two-photon states, one can quantify the entanglement by using a variety of entanglement measures [13, 14].

In this paper, we present a comprehensive framework of photonic state reconstruction and entanglement quantification that takes into account fiber attenuation. In

our model, the number of photons that successfully pass through the fiber is represented by a binomial distribution. Then, the shot noise related to photon-counting is imposed to make the scheme realistic. These assumptions allow us to study the efficiency of state tomography for various settings. The fidelity of quantum states is used as an indicator of the precision of state recovery. As for entanglement quantification, we implement two measures – the concurrence, which relates to two-qubit states, and the negativity, which works well for two-qutrit states.

In Sec. II, we introduce the framework, starting from the measurement scheme and noise model. Then, entanglement measures are defined. Next, in Sec. III, we present and discuss the results devoted to qubit tomography. Finally, in Sec. IV, we show the figures concerning qutrits. The findings of the article provide valuable insight into the impact of fiber attenuation on state tomography and entanglement detection. The work is concluded in the final section, where we also indicate possible problems for future research.

II. METHODS OF STATE ESTIMATION AND ENTANGLEMENT QUANTIFICATION

A. Quantum state tomography

To reconstruct an unknown photonic state, we implement a measurement scheme that is based on symmetric informationally complete positive operator-valued measures (SIC-POVMs) [15, 16]. For qubit tomography, the SIC-POVM involves four measurement operators, whereas, for qutrits, nine operators are required [17]. To estimate the state of entangled qubits, we construct 16 two-qubit measurement operators by implementing the tensor product. Analogously, for entangled qutrits, we obtain 81 operators,

In general, let us denote the measurement operators by: M_1, \dots, M_η , where η indicates the necessary number of operators. Then, we assume that the source gener-

* aczerwin@umk.pl

ates a beam containing \mathcal{N} photons (or photon pairs) per measurement. The photons are prepared in an identical quantum state that is described by a density matrix ρ_x . This allows one to write a formula for the expected photon count:

$$e_k = \lceil \mathcal{N} \text{Tr} M_k \rho_x \rceil, \quad (1)$$

where the symbol $\lceil a \rceil$ denotes rounding a to the nearest integer since the number of photons cannot be fractional. The density matrix ρ_x remains unknown to the observer and, for this reason, we follow the Cholesky decomposition to parameterize it depending on its dimension, cf. [18, 19].

The formula Eq. (1) models the photon counts according to the Born rule, which is a theoretical foundation for this measurement scheme. However, in practice, any act of measurement involves errors and uncertainty, which implies that the values provided by the detection system will be different from what one may expect. In quantum optics, we encounter the shot noise that describes the fluctuations of the number of photons counted by the system [20]. As a result, the measured counts are statistically independent Poissonian random variables. Thus, for an input state ρ_{in} , we simulate an experimental scenario by selecting measured counts randomly from a Poisson distribution: $m_k \in \text{Pois}(n)$ with the mean value given by

$$n = \lceil \tilde{\mathcal{N}} \text{Tr} M_k \rho_{in} \rceil, \quad (2)$$

where $\tilde{\mathcal{N}}$ represents the number of photons that reached the detection system after passing through the fiber. The value of $\tilde{\mathcal{N}}$ is generated randomly by taking into account fiber attenuation. According to the Beer–Lambert law, if the source generates a beam with the initial power P_0 that is transmitted through a fiber of the length L , the receiver gets the output power that can be expressed as

$$P_{out} = P_0 e^{-\frac{\alpha L}{10}}, \quad (3)$$

where α stands for the attenuation coefficient that characterizes the fiber. Conventionally, α is given in db/km. If we implement this law in the single-photon framework, it implies that a photon can be successfully passed through the fiber with probability $e^{-\frac{\alpha L}{10}}$ whereas $1 - e^{-\frac{\alpha L}{10}}$ gives the probability of a failure (photon loss). Consequently, number of photons that reach the receiver (out of the initially produced \mathcal{N}) can be modeled by the binomial distribution, i.e., $\tilde{\mathcal{N}} \in \mathcal{B}(\mathcal{N}, e^{-\frac{\alpha L}{10}})$. Similarly, for a two-photon state, we assume that the source generates \mathcal{N} photon pairs per measurement, and each of them travels through a separate fiber. Since we are interested in detecting coincidences, both photons need to arrive at the corresponding detector. Consequently, for two-photon states, the number of photon pairs that reach the detection system can be modeled as: $\tilde{\mathcal{N}} \in \mathcal{B}(\mathcal{N}, e^{-\frac{\alpha_1 L_1 + \alpha_2 L_2}{10}})$.

The above-described approach allows one to numerically generate photon counts that correspond to a realistic scenario for any input density matrix ρ_{in} . Then,

we follow the method of least squares (LS) to determine how well one can reconstruct the density matrix in spite of the uncertainty, cf. [21]. This means that we search for the minimum value of the function:

$$f_{LS}(t_1, t_2, \dots) = \sum_k (e_k - m_k)^2, \quad (4)$$

where t_1, t_2, \dots denote the set of real parameters that characterize the density matrix ρ_x .

To evaluate the performance of QST in the presence of fiber attenuation, we compute, for any input density matrix, its fidelity with the result of estimation [22]:

$$F[\rho_{in}, \rho_x] := \left(\text{Tr} \sqrt{\sqrt{\rho_{in}} \rho_x \sqrt{\rho_{in}}} \right)^2. \quad (5)$$

The efficiency of the framework depends on the properties of the input state. Therefore, to find an indicator of the average performance, we first select a sample of input states, then each of them undergoes the procedure of QST, and, finally, the average fidelity for the sample is computed. Additionally, we calculate sample standard deviation (SD) to quantify the statistical dispersion. In our study, the length of the fiber is considered an independent variable, which implies that the average fidelity can be treated as a function of L and denoted by $F_{av}(L)$. As a result, this figure of merit can be plotted to observe how the efficiency of QST changes as we increase L .

B. Entanglement quantification

Apart from evaluating the precision of state tomography, we also quantify the amount of entanglement detected by the scheme. For two-qubit states, we implement the concurrence, which can be computed directly for any density matrix ρ_x obtained from the scheme [23, 24]. The concurrence is an entanglement monotone, which gives $C[\rho] = 0$ for a separable state ρ , and $C[\rho] = 1$ for ρ representing a maximally entangled state. This figure of merit is commonly used to quantify entanglement with imperfect measurements [25, 26].

In our application, we consider entangled photon pairs such that each photon can travel through a fiber of a different length. Thus, for the reconstructed two-qubit state, we compute the concurrence, treating the fiber lengths as independent variables. Finally, the average concurrence for a sample of input states, denoted by $C_{av}(L_1, L_2)$, can be plotted like a two-variable function. This approach allows us to observe the quantity of entanglement embraced by the reconstructed states for different combinations of fiber lengths.

As for two-qutrit states, we utilize the negativity, which is a measure of quantum entanglement that can be relatively convenient for an arbitrary bipartite system [27]. For a density matrix ρ_x obtained from the scheme, we compute

$$N[\rho_x] = \frac{\|\rho_x^{\Gamma_A}\|_1 - 1}{2}, \quad (6)$$

where $\rho_x^{\Gamma_A}$ denotes the partial transpose of ρ_x with respect to the subsystem A and $\|\sigma\|_1$ represents the trace norm of σ , i.e., $\|\sigma\|_1 := \text{Tr}\sqrt{\sigma^\dagger\sigma}$. The formula Eq. (6) can be implemented numerically to allow for straightforward entanglement quantification. It is worth stressing that negativity is an entanglement monotone, but it does not always guarantee entanglement detection since, for PPT entangled states, it results in zero. However, in our framework, we operate with a sample of maximally entangled qutrits, which implies that negativity can be considered a proper entanglement measure. In the same vein as with the concurrence, we compute the average negativity for a sample and plot it as a two-variable function, denoted by $N_{av}(L_1, L_2)$.

III. QUBIT TOMOGRAPHY

A. Single qubits

First, we consider the efficiency of QST for single qubits. We selected a sample consisting of 220 pure states that are distributed uniformly on the Bloch sphere. Then, each input state goes through the framework, and the average fidelity is computed. In Fig. 1, one finds the results presenting $F_{av}(L)$, for three numbers of photons per measurement. The result correspond to a fixed attenuation coefficient: $\alpha = 0.2$ dB/km.

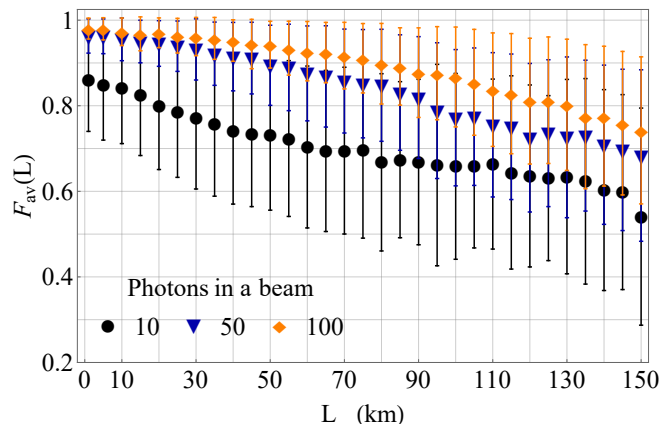


FIG. 1: Fidelity of qubit tomography, $F_{av}(L)$, for three numbers of photons per measurement. The attenuation coefficient is fixed: $\alpha = 0.2$ dB/km

From Fig. 1, one can observe how the quality of state recovery degenerates as we increase the fiber. A longer fiber involves more attenuated photons, which reduces the precision of measurements due to the shot noise. If we compare $\mathcal{N} = 50$ and $\mathcal{N} = 100$, we notice that initially, both settings provided similar accuracy. However, as we increase the fiber, the setting with 100 photons per measurement outperforms the other scenario. Also, one should notice that SD grows along with the fiber, which implies that the sample features more statistical

dispersion. Finally, for $\mathcal{N} = 10$, we see that even at the beginning, one is not able to properly estimate the state. Moreover, for 10 photons per measurement, the results are more scattered, which means we cannot predict the efficiency for a particular state.

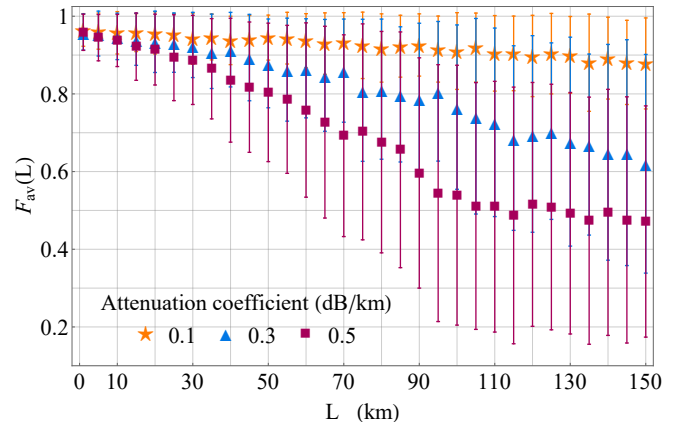


FIG. 2: Fidelity of qubit tomography, $F_{av}(L)$, for three attenuation coefficients. The number of photons per measurement is fixed: $\mathcal{N} = 50$.

Next, we consider $F_{av}(L)$ for three different attenuation coefficients while the number of photons is fixed: $\mathcal{N} = 50$. The findings are presented in Fig. 2. For $\alpha = 0.1$ dB/km, we witness stable precision of state estimation since the function decreases slowly. The results demonstrate that in this scenario, the framework is efficient even for longer fibers.

Then, for $\alpha = 0.3$ dB/km, we observe that the fidelity declines linearly as we increase the fiber. There are some irregularities in the plot, which can be attributed to the randomness of noise that affects the measurements.

Lastly, if $\alpha = 0.5$ dB/km, the fidelity reduces rapidly. For $L = 105$ km, we obtain $F_{av}(105 \text{ km}) = 0.52 \pm 0.32$, and then its value remains more or less constant. This observation suggests that one cannot efficiently estimate a qubit state in such conditions.

B. Entangled qubits

In this part, we apply the framework to one class of entangled qubits. More specifically, we investigate a following family of two-qubit states:

$$|\Phi(\phi)\rangle = \frac{1}{\sqrt{2}} (|0\rangle \otimes |0\rangle + e^{i\phi} |1\rangle \otimes |1\rangle), \quad (7)$$

where $\{|0\rangle, |1\rangle\}$ represents the standard basis in the two-dimensional Hilbert space and $0 \leq \phi < 2\pi$. We select a sample of 100 states of the form Eq. (7) such that the relative phase ϕ covers the full range.

We focus on this particular class of two-qubit entanglement since it comprises the celebrated Bell states, i.e.,

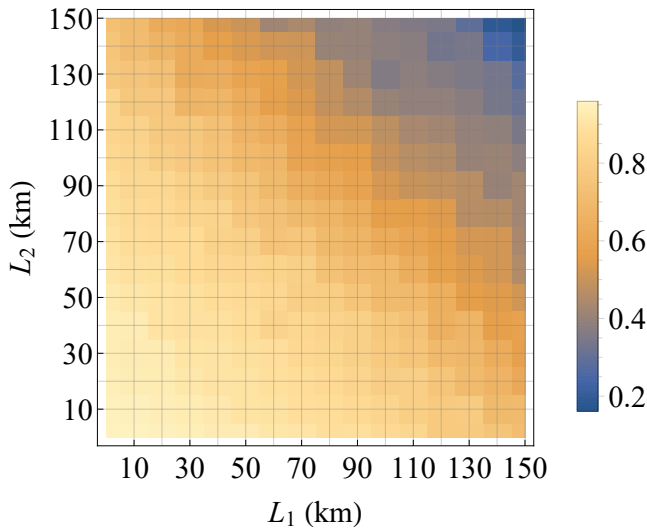


FIG. 3: Fidelity of entangled qubits tomography, $F_{av}(L_1, L_2)$. The number of photon pairs per measurement is fixed: $\mathcal{N} = 200$ and attenuation coefficient is $\alpha = 0.2$ dB/km.

$|\Phi^+\rangle$ and $|\Phi^-\rangle$, which are famous for multiple applications in quantum information and computation. In quantum optics, such kind of two-photon entangled states can be produced by spontaneous four-wave mixing (SFWM) in a dispersion-shifted fiber [28], or spontaneous parametric down-conversion (SPDC) [29], and by a source that utilizes quantum dots [30].

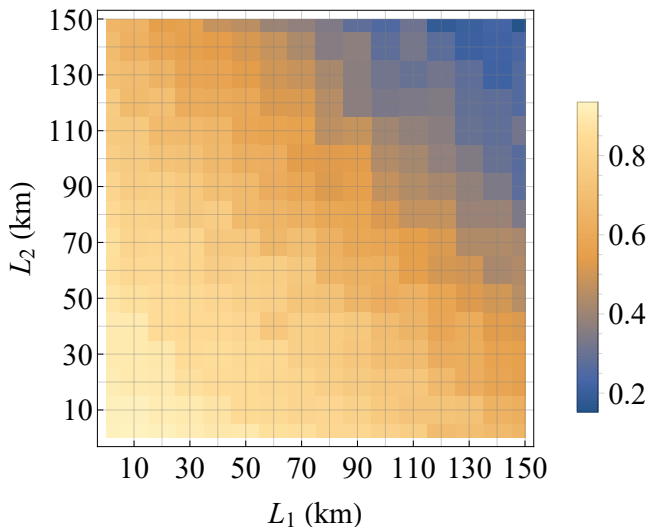


FIG. 4: Concurrence of entangled qubits tomography, $C_{av}(L_1, L_2)$. The number of photon pairs per measurement is fixed: $\mathcal{N} = 200$ and attenuation coefficient is $\alpha = 0.2$ dB/km.

In Fig. 3, one finds the average fidelity, $F_{av}(L_1, L_2)$, corresponding to entangled qubits estimation. The map allows one to follow the precision of state reconstruction

for different combinations of fiber lengths. We assumed that the number of photon pairs per measurement and the attenuation coefficient remained unchanged.

Furthermore, in Fig. 4, we present the average concurrence, $C_{av}(L_1, L_2)$, which corresponds to the estimated states. Originally, all input states were maximally entangled with concurrence equal to one. However, as a consequence of photon loss and shot noise, the measured states feature less entanglement. The plot Fig. 4 allows one to track how the quantity of entanglement detected by the measurement scheme depends on fiber lengths.

For practical reasons, we are usually interested in detecting such quantity of entanglement that is sufficient to announce the violation of the Bell-CHSH inequality [31, 32]. Based on the concurrence, we can say that a quantum state ρ allows of such a violation if $C[\rho] > 1/\sqrt{2}$ [33, 34]. From Fig. 4, one can conclude that $C_{av}(L_1, L_2) > 1/\sqrt{2}$ as long as $L_1 + L_2 < 130$ km. This observation provides us with a threshold for detecting quantum correlations. By following the framework introduced in this work, one can determine an analogous criterion for a different number of photon pairs or distinct attenuation coefficient.

IV. QUTRIT TOMOGRAPHY

A. Single qutrits

In addition, we examine the performance of the QST framework with single qutrits. We took sample of 5184 pure qutrit states, which are equidistant across all parameters of the general representation of a qutrit pure state [35]. Each input state sequentially passes through the framework, and the average fidelity is calculated. In Fig. 5, we present the results of the average fidelity calculation, $F_{av}(L)$, for three numbers of photons per measurement: $\mathcal{N} = 10, 50$, and 100 . The results are estimated for a fixed attenuation coefficient: $\alpha = 0.2$ dB/km.

For two cases: $\mathcal{N} = 50$ and $\mathcal{N} = 100$, the results presented in Fig. 5 demonstrate that if we increase the fiber length, one can observe that the average fidelity, $F_{av}(L)$, drops down nearly linearly. Deformation of the estimated state is caused by the absorption, which decreases the number of photons in measurements. Comparing these findings with qubits, we do not observe a big difference. The scenario for $\mathcal{N} = 50$ shows a more noticeable linear decreasing of $F_{av}(L)$ with longer fiber. Similar behavior of the average fidelity is observed for the qubits, but the slope of the qutrit curve is more significant. It can be concluded that it needs more measurements to achieve good fidelity for a higher dimensional state. It stems from the need to estimate more parameters. Moreover, we can observe that the standard deviation increases with the length of the fiber.

Then, we considered the properties of $F_{av}(L)$ for a constant number of photons: $\mathcal{N} = 50$, and three different attenuation parameters: $\alpha = 0.1, 0.3$ and 0.5 dB/km.

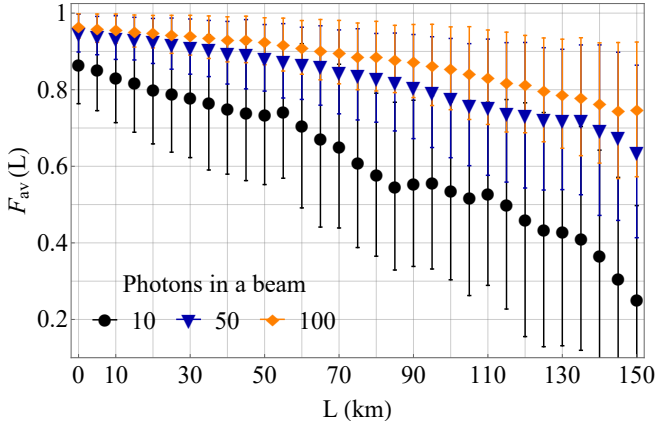


FIG. 5: Fidelity of qutrit tomography, $F_{av}(L)$, for three numbers of photons per measurement. The attenuation coefficient is fixed: $\alpha = 0.2$ dB/km.

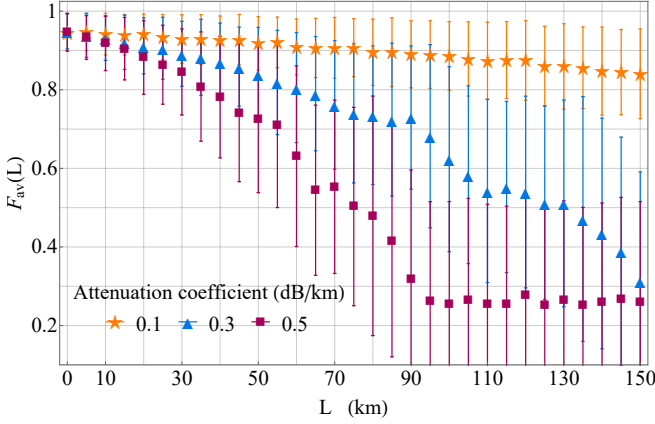


FIG. 6: Fidelity of qutrit tomography, $F_{av}(L)$, for three attenuation coefficients. The number of photons per measurement is fixed: $\mathcal{N} = 50$.

We observe faster degradation of state estimation for an increased damping factor. The trend of the decrease of the average fidelity is linear for 0.1 and 0.3 dB/km. This behavior is no longer valid for the highest attenuation coefficient $\alpha = 0.5$ dB/km. First, we witness a rapid decline in the accuracy of state estimation. Later, for $L \geq 95$ m, the function $F_{av}(L)$ stabilizes and maintains roughly a constant value. This feature is analogous to the characteristics of $F_{av}(L)$ observed for qubits for the same parameters, see Fig. 2. However, in the case of qutrits, the constant value of $F_{av}(L)$ is lower than in the case of qubits. This implies that a long fiber combined with a higher attenuation coefficient is highly detrimental to a qutrit state recovery.

B. Entangled qutrits

To study the performance of QST for entangled qutrit states, we chose a class of maximally entangled states:

$$|\Theta(\phi)\rangle = \frac{1}{\sqrt{3}} (e^{i\phi} |0\rangle \otimes |2\rangle + |1\rangle \otimes |1\rangle + e^{i\phi} |2\rangle \otimes |0\rangle), \quad (8)$$

where $\{|0\rangle, |1\rangle, |2\rangle\}$ represents the standard basis in the three dimensional Hilbert space and $0 \leq \phi < 2\pi$. The sample consists of 100 states equally spaced due to the relative phase ϕ . We selected the input states $|\Theta(\phi)\rangle$ since such systems can be easily produced with a spatial degree of freedom in the SPDC process [36].

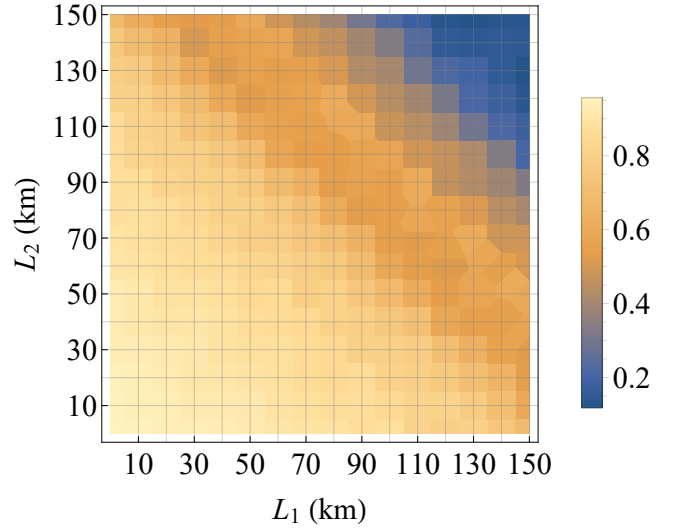


FIG. 7: Fidelity of entangled qutrits tomography, $F_{av}(L_1, L_2)$. The number of photons pairs per measurement is fixed: $\mathcal{N} = 200$ and the attenuation coefficient is $\alpha = 0.2$ dB/km.

In Fig. 7, we display the average fidelity depending on lengths of two fibers, with $\mathcal{N} = 200$ and the attenuation coefficient: 0.2 dB/km. The state deformation becomes larger as the lengths of the optical fibers increase in both arms. However, it can be observed that when only in one channel fiber length increases, we are still getting a reliable state estimation.

In Fig. 8, we present the mean negativity, which represents the amount of entanglement of the reconstructed two-qutrit state after the transmission in fibers in two arms. The simulations were performed for $\mathcal{N} = 200$ and attenuation coefficient 0.2 dB/km. The amount of entanglement will decrease monotonically as the optical fiber length becomes greater in both directions. Similarly to the fidelity case, the measurement of negativity gives a high amount of entanglement when one party has a long fiber, and the other uses a short channel. Due to the necessity to estimate many parameters, the performance for entangled qutrits is more distorted by the absorption in optical fibers than in the qubit case. Moreover,

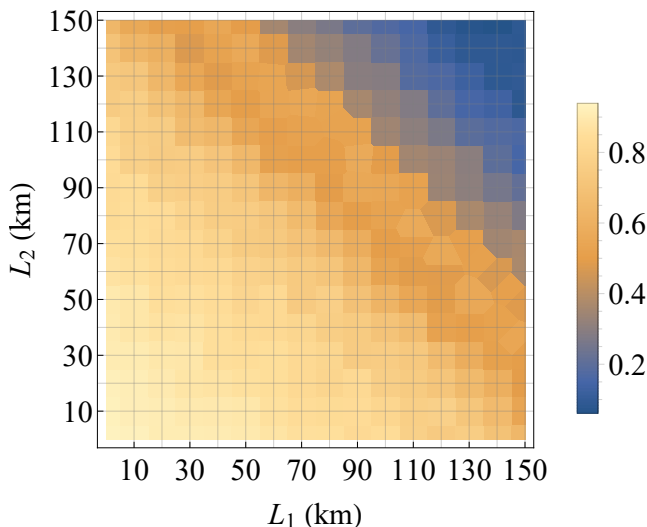


FIG. 8: Negativity of entangled qutrits tomography, $N_{av}(L_1, L_2)$. The number of photon pairs per measurement is fixed: $\mathcal{N} = 200$ and the attenuation coefficient is $\alpha = 0.2$ dB/km

the negativity measurement for the employed sample of states with deformation stemming from the absorption in fiber is well-behaving. Minor inaccuracies that occurred in Fig. 8 (e.g., the function $N_{av}(L_1, L_2)$ is not always monotone) can be attributed to the random nature of noise.

V. CONCLUSIONS AND OUTLOOK

In this paper, we have demonstrated a framework of QST that incorporates the effects of fiber attenuation. The binomial distribution was implemented to model the number of photons that successfully pass through the fiber. Moreover, the shot noise was added to simulate realistic photon counts.

The scheme was adapted to qubit and qutrit tomography, while special attention was paid to entangled states. With selected figures of merit, we could track both the precision of state reconstruction and quantity of entanglement detected by the framework. The results allow one to observe how the quality of transmission degenerates as we increase the fiber length. The findings of the paper may have relevant implications for future experiments. One needs to properly select the duration of a light pulse to guarantee a sufficient number of photons per measurement. In other words, the awareness of how fiber attenuation impacts transmission of photons will help an experimenter to adjust the input power of the source so that the detectors receive a satisfactory signal.

There are remaining open problems that can be addressed in forthcoming papers. Most of all, fluctuations of the source should be taken into account. Even if we tune the source to a specific power, the number of photons emitted in a single shot can vary. More specifically, it should not be treated as a constant value but rather as a random variable generated from a distribution that characterizes the source. Furthermore, apart from fiber attenuation, we should also consider scattering processes that occur during the transmission of photons and influence the detection. A thorough description of all factors that impact photonic tomography will lead to better understanding and, presumably, more effective practical implementations of quantum information protocols.

ACKNOWLEDGMENTS

A. C. acknowledges financial support from the National Science Centre in Poland, grant No. 2020/39/I/ST2/02922. J. S. was supported by the Foundation for Polish Science (FNP), project First Team co-financed by the European Union under the European Regional Development Fund, grant no. First Team/2017-3/20, and National Laboratory of Atomic, Molecular and Optical Physics.

-
- [1] S. Pirandola, U. L. Andersen, L. Banchi, M. Berta, D. Bunandar, R. Colbeck, D. Englund, T. Gehring, C. Lupo, C. Ottaviani, J. L. Pereira, M. Razavi, J. Shamsul Shaari, M. Tomamichel, V. C. Usenko, G. Vallone, P. Villoresi, and P. Wallden, *Adv. Opt. Photon.* **12**, 1012-1236 (2020).
 - [2] Ch. H. Bennett, G. Brassard, Quantum Cryptography: Public key distribution and coin tossing, in *n Proc. IEEE International Conference on Computers, Systems and Signal Processing*, Bangalore, India, pp. 175-179, (1984).
 - [3] Ch. H. Bennett, G. Brassard, *Theor. Comput. Sci.* **560**, 7-11 (2014).
 - [4] Ch. H. Bennett, F. Bessette, G. Brassard, L. Salvail, and J. Smolin, *J. Cryptology* **5**, 3-28 (1992).
 - [5] A. K. Ekert, *Phys. Rev. Lett.* **67**, 661 (1991).
 - [6] H.-L. Yin, T.-Y. Chen, Z.-W. Yu, H. Liu, L.-X. You, Y.-H. Zhou, S.-J. Chen, Y. Mao, M.-Q. Huang, W.-J. Zhang, H. Chen, M. J. Li, D. Nolan, F. Zhou, X. Jiang, Z. Wang, Q. Zhang, X.-B. Wang, and J.-W. Pan, *Phys. Rev. Lett.* **117**, 190501 (2016).
 - [7] J.-P. Chen, C. Zhang, Y. Liu, C. Jiang, W. Zhang, X.-L. Hu, J.-Y. Guan, Z.-W. Yu, H. Xu, J. Lin, M.-J. Li, H. Chen, H. Li, L. You, Z. Wang, X.-B. Wang, Q. Zhang, and J.-Wei Pan, *Phys. Rev. Lett.* **124**, 070501 (2020).
 - [8] X.-T. Fang, P. Zeng, H. Liu, M. Zou, W. Wu, Y.-L. Tang, Y.-J. Sheng, Y. Xiang, W. Zhang, H. Li, Z. Wang, L. You, M.-J. Li, H. Chen, Y.-A. Chen, Q. Zhang, Ch.-Z. Peng, X. Ma, T.-Y. Chen, and J.-W. Pan, *Nat. Photonics* **14**, 422-425 (2020).

- [9] W. K. Wootters and W. H. Zurek, *Nature* **299**, 802–803 (1982).
- [10] M. Paris and J. Řeháček (eds.), *Quantum State Estimation* (Springer, Heidelberg, 2004).
- [11] A. G. White, D. F. V. James, P. H. Eberhard, and P. G. Kwiat, *Phys. Rev. Lett.* **83**, 3103 (1999).
- [12] R. T. Horn, P. Kolenderski, D. Kang, P. Abolghasem, C. Scarcella, A. D. Frera, A. Tosi, L. G. Helt, S. V. Zhukovsky, J. E. Sipe, G. Weihs, A. S. Helmy, and T. Jennewein, *Sci. Rep.* **3**, 2314 (2013).
- [13] M. Horodecki, *Quantum Inf. Comput.* **1**, 3-26 (2001).
- [14] J. Eisert and M. M. Wilde, A smallest computable entanglement monotone, arXiv:2201.00835 (2022).
- [15] J. M. Renes, R. Blume-Kohout, A. J. Scott, and C. M. Caves, *J. Math. Phys.* **45**, 2171–2180 (2004).
- [16] Ch. A. Fuchs, M. C. Hoang, and B. C. Stacey, *Axioms* **6**, 21 (2017).
- [17] C. Paiva-Sánchez, E. Burgos-Inostroza, O. Jiménez, and A. Delgado, *Phys. Rev. A* **82**, 032115 (2010).
- [18] D. F. V. James, P. G. Kwiat, W. J. Munro, and A. G. White, Measurement of qubits, *Phys. Rev. A* **64**, 052312 (2001).
- [19] J. B. Altepeter, E. R. Jeffrey, and P. G. Kwiat, Photonic State Tomography, *Adv. At. Mol. Opt. Phys.* **52**, 105-159 (2005).
- [20] S. W. Hasinoff, Photon, Poisson noise, in *Computer Vision*, edited by K. Ikeuchi (Springer, Boston, MA, 2014), pp. 608-610.
- [21] A. Czerwinski, K. Sedziak-Kacprowicz, and P. Kolenderski, *Phys. Rev. A* **103**, 042402 (2021).
- [22] M. A. Nielsen and I. L. Chuang, *Quantum Computation and Quantum Information* (Cambridge University Press, Cambridge, 2000).
- [23] S. Hill and W. K. Wootters, *Phys. Rev. Lett.* **78**, 5022-5025 (1997).
- [24] W. K. Wootters, *Phys. Rev. Lett.* **80**, 2245-2248 (1998).
- [25] S. P. Walborn, P. H. Souto Ribeiro, L. Davidovich, F. Mintert, and A. Buchleitner, *Nature* **440**, 1022-1024 (2006).
- [26] L. Neves, G. Lima, E. J. S. Fonseca, L. Davidovich, and S. Padua, *Phys. Rev. A* **76**, 032314 (2007).
- [27] G. Vidal and R. F. Werner, *Phys. Rev. A* **65**, 032314 (2002).
- [28] H. Takesue and Y. Noguchi, *Opt. Express.* **17**, 10976 (2009).
- [29] I. Marcikic, H. de Riedmatten, W. Tittel, H. Zbinden, M. Legre, and N. Gisin, *Phys. Rev. Lett.* **93**, 180502 (2004).
- [30] H. Jayakumar, A. Predojevic, T. Kauten, T. Huber, G. S. Solomon, and G. Weihs, *Nat. Commun.* **5**, 4251 (2014).
- [31] J. S. Bell, *Physics Physique Fizika* **1**, 195 (1964).
- [32] J. F. Clauser, M. A. Horne, A. Shimony, and R. A. Holt, *Phys. Rev. Lett.* **23**, 880 (1969).
- [33] F. Verstraete and M. M. Wolf, *Phys. Rev. Lett.* **89**, 170401 (2002).
- [34] M.-L. Hu, *Quantum Inf. Process.* **12**, 229 (2012).
- [35] J Szlachetka, A Czerwinski, *Acta Phys. Pol. A* **140**, 210-214 (2021).
- [36] W. M. Pimenta, B. Marques, T. O. Maciel, R. O. Vianna, A. Delgado, C. Saavedra, and S. Padua, *Phys. Rev. A* **88**, 012112 (2013).